Time-resolved absorption spectroscopic characterization of ultrafast laser-produced plasmas under varying background pressures

S. S. Harilal, E. J. Kautz, and M. C. Phillips

Phys. Rev. E **103**, 013213 — Published 28 January 2021

DOI: 10.1103/PhysRevE.103.013213

Time-resolved absorption spectroscopic characterization of ultrafast laser-produced plasmas under varying background pressures

S. S. Harilal,[1] E. J. Kautz,[1] M. C. Phiilips[2]

[1]*Pacific Northwest National Laboratory, Richland, Washington 99354 USA*
[2]*James C. Wyant College of Optical Sciences, University of Arizona, Tucson, Arizona 85721 USA*

Time-resolved tunable laser absorption spectroscopy is used to characterize the physical properties of ultrafast laser-produced plasmas. The plasmas were produced from an Inconel target, with ≤ 0.4 wt. % Al, using ~ 35 fs, ~800 nm, ~5 mJ laser pulses at varying Ar background pressures from 1-100 Torr. The absorption spectrum of atomic Al is measured with high spectral and temporal resolution when the probe laser is stepped across the selected Al transition at 394.4 nm. Spectral fitting is used to infer linewidths, kinetic temperature, Al column density, and pressure broadening coefficient. The late time physical properties of plasmas are compared for various pressure levels. Our studies highlight that a significant lower state population exists even at early times of ultrafast laser-produced plasma evolution, and lower state population persistence decreases with increasing ambient pressure. We also show that the fundamental optical properties, such as pressure-broadening, can be measured using ultrafast laser-produced plasmas combined with laser absorption spectroscopy.

I. INTRODUCTION

When a powerful laser interacts with a solid target, the ablated material is transformed into plasma, which contains ions, atoms, molecules, and nanoparticles. These transient plasmas are used in numerous fields, most notably analytical applications [1,2]. The physics of laser-produced plasma (LPP) generation and its expansion is very complex and depends on several experimental parameters, including laser (intensity, wavelength, pulse width) and target properties and the nature and pressure of the ambient medium [1]. In the last decade, ultrafast 'femtosecond' lasers have gradually gained more widespread use and popularity, replacing traditional long pulse 'nanosecond' lasers for various LPP applications due to several advantages. Some of the documented benefits of using fs lasers over ns lasers for plasma production include reduced heat-affected zone (HAZ), nanoparticle generation, lesser matrix effects, a reduced continuum in emission features, early time molecular formation, and more [2-5]. Besides, ultrafast laser pulses have a lower ablation threshold (laser fluence) and generate a lower temperature plasma due to the lack of laser-plasma coupling [6].

A background gas is typically used for studying LPPs, although the nature and pressure of the gas vary with each application [7,8]. However, the interaction of an LPP with a background gas is very complicated due to the multiple inter-related processes such as shock wave formation, plume splitting and sharpening, deceleration, confinement, and thermalization of ablated species, diffusion, plume chemistry, etc. [7,9]. LPPs expand freely in a vacuum and low-pressure environment. The plume-ambient collisional effects become dominant at moderate pressure levels when the mean free path of the ambient medium approaches the Debye length of the plasma particles. The presence of moderate background gas pressure (1-100 Torr) helps to extend the lifetime of the LPP by regulating the rapid decay of temperature and density. However, an additional increased pressure leads to effective plume confinement, which promotes rapid cooling of the plasma plume because of the enhanced collisions, reducing the persistence of

the LPP. The selection of the background gas also influences the LPP properties. For e.g., the presence of an inert gas environment (Ar, He, etc.) inhibit any plasma chemistry typically seen in the presence of reactive gases such as air [10,11].

Plasma diagnostics play an essential role in optimizing LPPs for various applications. In addition to its use in analytical applications, optical spectroscopic tools can be used for measuring important plasma physical properties such as the density of species (e.g., atom, ion, electron, etc.), temperature, ionization fraction, and more [12-15]. Although all-optical spectroscopic tools, viz. laser absorption spectroscopy (LAS), optical emission spectroscopy (OES), and laser-induced fluorescence (LIF) are well suited for analytical applications and plasma characterization, OES (commonly called laser induced breakdown spectroscopy or LIBS) is more widely used due to the simplicity of the required experimental set-up [1,2]. However, the emission from LPP plumes depends on electronic excitation, which occurs only when the temperature of the plasma is higher and hence is short-lived. In contrast, both absorption and fluorescence spectroscopy use lower state populations of atoms or ions that can be probed when the plasma is cooler and persists for very long times [1,16-22]. Further, both LAS and LIF provide improved analytical merits compared to emission spectroscopy [23,24]. LAS is also less sensitive to the effects of self-absorption and self-reversal which can complicate analysis of LA plumes via OES. LAS employing narrow-linewidth tunable lasers is also immune to instrumental broadening seen in OES set up and hence provides high spectral resolution [1,17]. The recorded spectral profiles can also be used for temperature measurement through Doppler broadening and column density of selected atoms. Hence, LAS is uniquely suited to measure the properties at all times throughout LPP evolution and can provide important information on chemical dynamics, including molecular formation and particle condensation.

Although there exist numerous articles on the physical characterization of LPPs at early times of its evolution employing various diagnostic tools [2,14,25-31], there is only limited work evaluating the LPP's physical conditions at later times [18,20,32,33], even for ns LPP. This lack of data is partly due to the inability of most plasma diagnostics to characterize low-temperature and low-density plumes. However, the knowledge of lower-state population of various species at early and late times, particularly in the presence of a background gas medium, is essential for gaining insight into molecular, aerosols, and particulate formation mechanisms in plasmas and fireballs. In this article, we used high-resolution time-resolved LAS for the comprehensive characterization of ultrafast LA plumes during its entire lifecycle. We evaluated the plasma properties at varying background Ar pressures ranging from 1-100 Torr. Time-resolved Al atomic absorption spectral features were recorded for times 1-500 μs after plasma onset. Spectral fitting using Voigt profiles was performed for measuring linewidths and inferring time-resolved physical properties of plasmas, including kinetic temperature, path-integrated atomic number densities, and optical properties such as pressure broadening coefficient.

II. EXPERIMENTAL

The schematic of the experimental setup is given in Fig. 1. The ablation laser used in these experiments was a Ti:Sapphire Coherent Astrella, providing ~ 35 fs pulses, ~ 800 nm pulses. A combination of a halfwave plate and thin-film polarizer was used for controlling laser energy at the target. The laser energy and repetition rate used for ablation in our experiments was ~ 5 mJ and 10 Hz. The spot size and laser fluence at the target were ~ 200 μm and 15 J/cm^2, respectively. The selected laser energy and fluence are typical values used for various analytical applications of fs LPP. An Inconel (i.e. Ni-Cr-Fe-Mo alloy) target with ~0.4 wt. % Al was used for ablation. The target was mounted in a cubic vacuum chamber, which contained transmission windows for ablation and probe laser

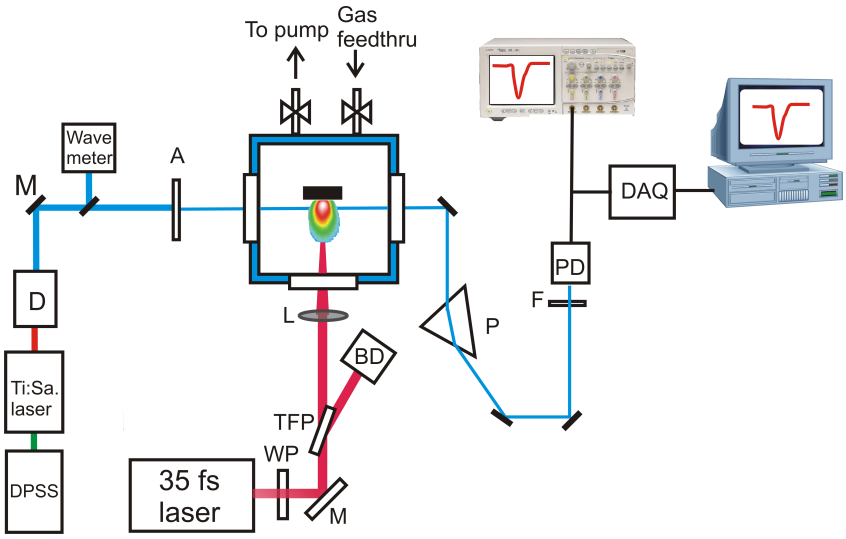

FIG. 1. Schematic of the experimental set up. Acronyms are defined as follows: DPSS – 532 nm diode pumped solid state laser, D -frequency doubler, M- mirror, A - attenuator, BD – beam dump, TFP – thin film polarizer, WP – wave plate, fs – femtosecond, P – prism, F – filter, PD – photodiode , DAQ – Data acquisition device.

entrance, ports for pumping, gauge, and gas feed-through. The chamber was positioned on a motorized X-Y translation stage so that target can be moved during ablation events. All experiments were performed in an Ar background gas (99.99 % purity), and the Ar pressure was varied from 1-100 Torr.

The probe laser was a frequency-doubled tunable Ti:Sapphire laser (M-squared), which provided wide tunability and wavelength selection with a linewidth ≤ 100 kHz. The probe laser with ~1 mm diameter was directed through the plasma ~ 0.75 mm from the target. The frequency of the probe laser was monitored using a wavemeter. The selected transition for the present study is Al I 394.401 nm ($3s^2 4s\ ^2S_{1/2} \rightarrow 3s^2 3p\ ^2P^o_{1/2}$, 0 - 25,347.756cm^{-1},), which is a strong resonance transition (gf = -0.623) and provides a good absorbance signal to noise ratio (SNR) even at very late times of plasma lifecycle. In addition to these, all spectroscopic information of the selected transition is readily available [34]. The probe laser wavelength is scanned across the selected transition over ~25 GHz for recording the absorption features. After passing through the ablation plume, the probe laser was directed through a prism and a series of bandpass and absorptive filters and detected using a Si photodiode with 200 ns rise time. The signal was digitized using a 16-bit ADC at a 2 MHz sampling rate. A LabVIEW program was written for real-time analysis of the time-resolved absorbance and absorption spectrum.

III. RESULTS AND DISCUSSION

Time-resolved probe transmission was recorded as the frequency of the probe laser was stepped across the Al I transition at 394.4 nm, and the measurement was averaged over six laser shots for each frequency step. The recorded probe transmission $I(f,t)$ was then converted to absorbance via $A(f,t) = -\ln[I(f,t)/I_0(f)]$ where $I_0(f)$ is the average of the transmitted intensity over the 5 μs before the ablation event. The acquired data for each probe scan was converted to a map of absorbance versus probe laser frequency and time after plasma onset, and

results are given in Fig. 2 for the following Ar background pressure levels: 1.1, 6, 13.7, 45, and 100 Torr. Please note that the time range (y-axis) given for various pressure levels is different in the sub-figure for clarity, although the data set was recorded up to 1 ms for each pressure. The temporal evolution of absorbance when the probe laser is in resonance with Al I peak center is given in Fig. 2f for various pressure levels. Laser absorption spectroscopy is a very sensitive technique. Although the laser pulse (~35 fs) used for producing plasmas are termed as 'ultrafast', the absorption signal from plasma is observed for several hundred microseconds (Figure 2).

Our previous experiments with pure metal targets showed high atomic density at early times (≤ 50 μs), leading to low transmission at the line center, and as a result, the absorption lineshape near the peak center cannot be determined with high accuracy [17,35]. Inconel contains Al as a minor alloying element, and hence results in lower peak absorbances. All experiments were performed in an Ar background gas in the pressure range of 1-100 Torr. At lower pressure levels, the absorption signal levels are lower due to free expansion of the plume, and hence. Similarly, at high pressures (e.g., atmospheric pressure conditions), the turbulence/instability in the plasma leads to poor SNR. The selection of Ar background gas also helps to mitigate plasma chemistry (e.g., oxidation reactions). Previous studies showed that the presence of plume chemistry would reduce plasma persistence significantly [36].

The 2D time-resolved absorption spectra (TRAS) profiles given in Fig. 2 contain several interesting observations, including (i) the peak absorbance increases with pressure; (ii) peak absorbance is shifted in time with increasing pressure; (iii) the absorbance persistence is reduced for higher pressures; (iv) a dual peak absorbance distribution is observed at moderate pressure levels (6-14 Torr range); (v) the absorption spectra are broadened at early times regardless of background pressure levels and (vi) The spectral broadening at late times increases for higher background pressure levels.

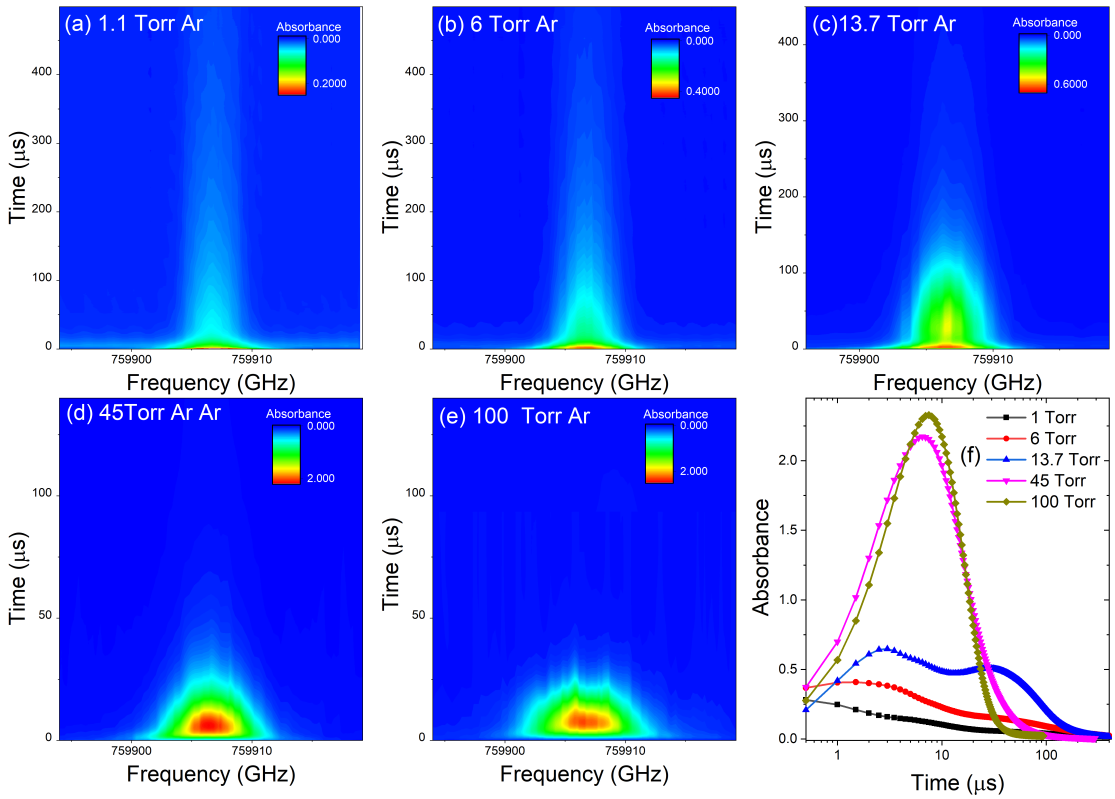

Fig. 2. 2D contours showing TRAS for Al I transition at 394.401 nm for the following Ar background pressures: (a) 1.1 Torr, (b) 6 Torr, (c) 13.7 Torr, (d) 45 Torr and (e) 100 Torr. The temporal evolution of absorbance is given in (f) when the probe laser is in resonance with Al line center. The spectra were acquired at a distance ~0.75 mm from the target surface, with the ablation laser fluence ~15 J/cm^2.

At each time and pressure, experimental spectra were fit using Voigt profiles to determine the peak areas, peak center frequency, Lorentzian linewidth, and Gaussian linewidth. A spectrally flat baseline was also included in the fit. Representative fits are given in Fig. 3 for select times and all background pressures. For fitting the absorbance spectra, due to the presence of the hyperfine structure of the ^{27}Al transition, it was modeled using sums of Voigt functions for accounting for the hyperfine structures [37,38]. Neglecting their effect on the spectral lineshape leads to additional errors in the linewidth and kinetic temperature measurement. The entire ^{27}Al hyperfine manifold was adjusted in center frequency and the total area to best fit the experimental Al absorption spectrum. Al hyperfine structures are very closely spaced, and hence it is not possible to resolve in the present study due to other broadening mechanisms in the plasma (e.g., Doppler, Stark). The SNR of the experimental data is excellent, and good fits to the model spectra were obtained except at early times and at the extreme end of the plume lifecycle (e.g., $\geq$ 500 μs for 1 Torr). At early times, due to large gradients in the plasma (i.e., spatial inhomogeneities), the spectral profile deviated from the Voigt profile. Furthermore, the spectral profile was broadened significantly, and ascertaining the baseline was difficult.

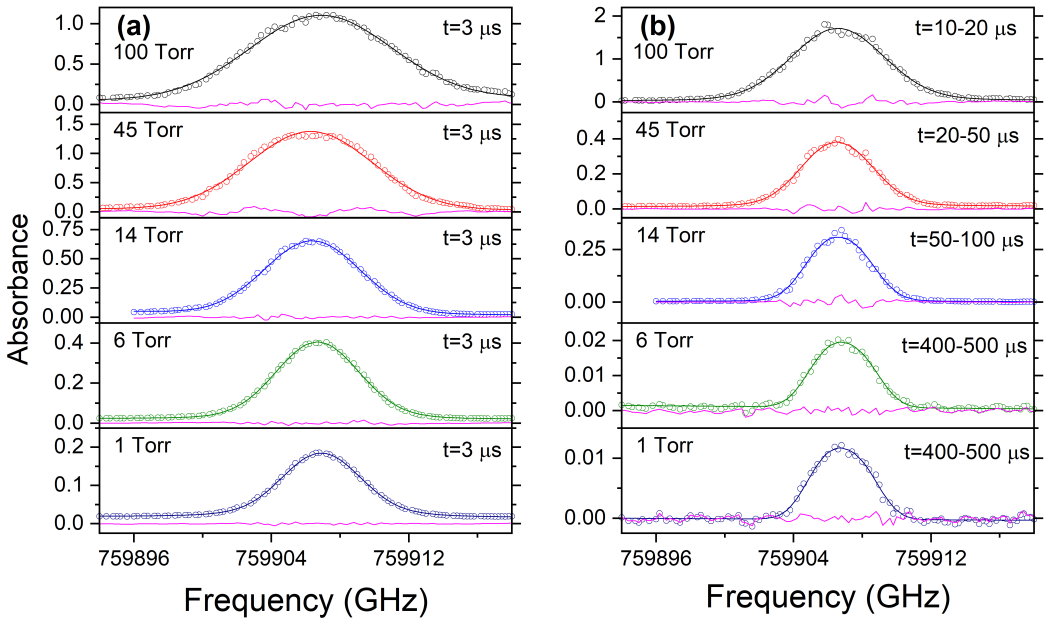

Fig.3 Measured absorption spectra (open circles), best fit spectra (solid lines), and fit residuals (magenta lines) for various times and pressures. (a) t = 3 μs, no averaging. (b) Averages over times shown in figures.

The measured time evolution of linewidths (FWHM) of Al transition for various background pressures are given in Fig. 4. Note that the linewidth plotted is for each hyperfine transition, and not the total observed linewidth from the sum over all hyperfine transitions. Regardless of the Ar pressure, the linewidths are initially broad but decrease rapidly as the plume expands and cools; however, the decay rate is noticeably faster with increasing background gas pressure. The Voigt linewidths for all background pressure are approaching ~4-5 GHz at times ≥10 μs and reduction in linewidth at later times are smaller. The early-time line broadening is also found to increase with pressure, and maximum linewidth is observed for the highest pressure studied here (100 Torr).

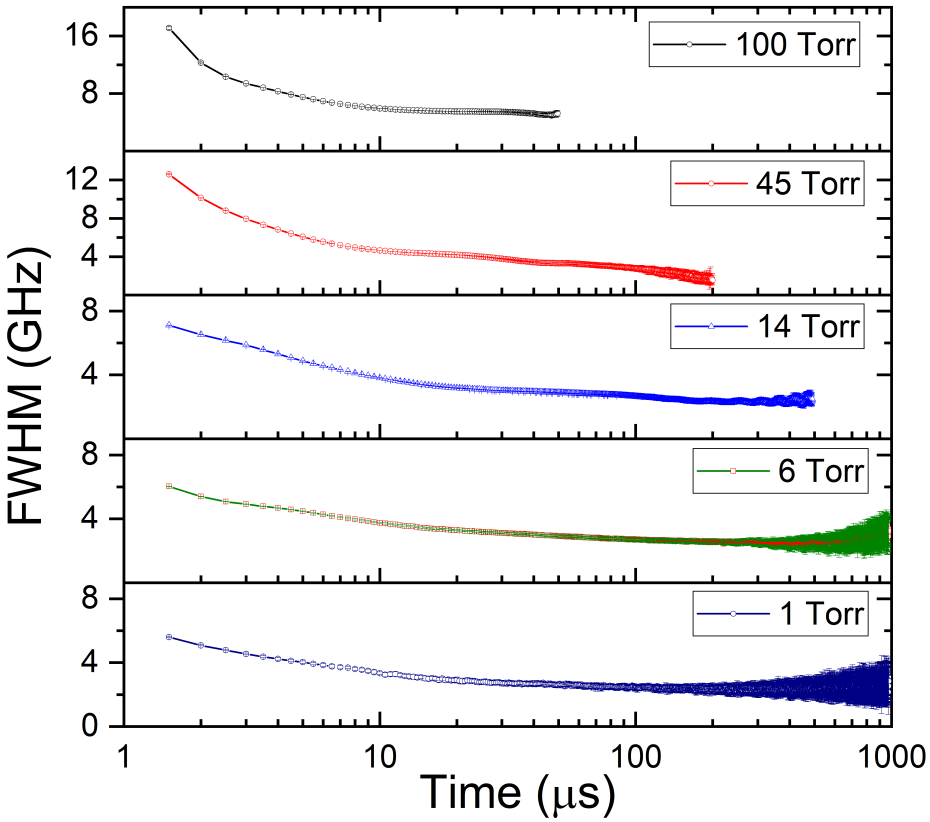

Fig. 4. Time resolved linewidth (FWHM) as a function of Ar background pressure.

The path-integrated lower state number density, or column density, n_1L for Al is calculated using $\int \alpha(\nu)L\, d\nu = 2.654 \times 10^{-6}[m^2/s] \cdot f_{12}n_1L$, where the left-side of the equation is the spectrally integrated absorbance as determined from the peak areas, f_{12} is the oscillator strength of the measured transition, n_1 is the number density of the lower state, and L is the path length [37]. The measured time evolution of column density for various pressure levels are given in Fig. 5. The column densities are found to increase with pressure at early times, but decay rapidly with increasing pressure.

The variation in measured linewidths with pressure and time is due to changes in the physical conditions of the plasma. All spectral lines in an LPP undergo various types of broadening mechanisms, and hence the measured spectral profiles can be used to infer some of the fundamental properties of the plasma. Among them, the Stark and Doppler broadening mechanisms are the major contributors to the LPP linewidth variations [1]. The Stark effect is contributed by charged particles and will be predominant at early times, and its contribution becomes negligible at times ≥ 3 μs. The Doppler effect, contributed by the thermal motion of species with respect to the observer, will become the dominant contributor at later times of plasma evolution when the plasma expands in a moderate-pressure ambient gas environment. The Stark effect provides a Lorentzian profile, whereas the Doppler effect gives a Gaussian distribution. Other broadening mechanisms include van der Waals and resonance broadening, although their effects are lesser than Stark and Doppler except in conditions of high pressure and/or atomic number density [1,39]. Hence, the measured spectral shapes are due to the convolution of multiple mechanisms and can, therefore, be accurately represented by Voigt profiles.

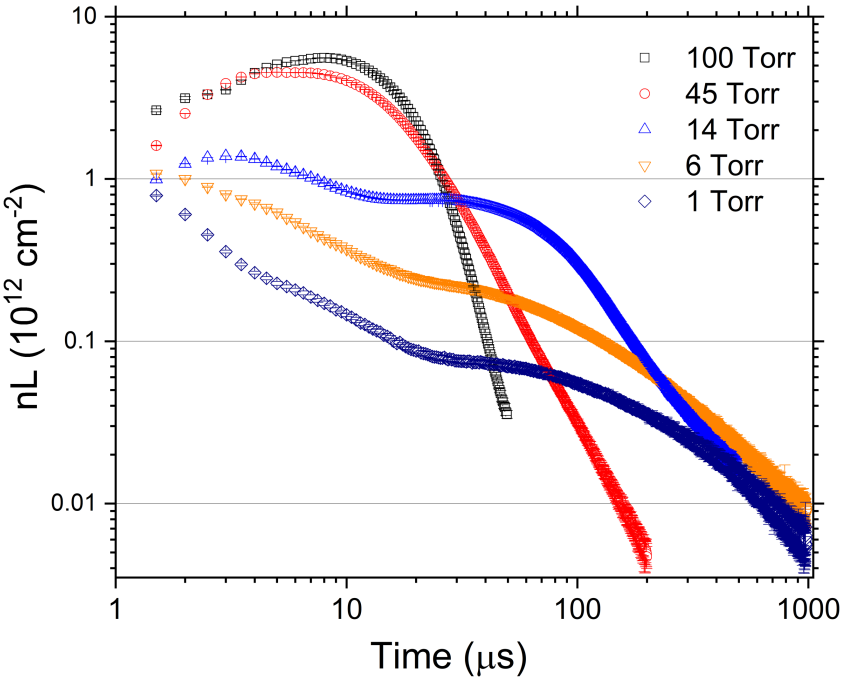

Fig. 5. The time evolution of path-integrated Al atom density (nL) for Ar pressures between 1 and 100 Torr.

The kinetic temperature, T_k, is calculated from the Gaussian widths using the relation: $T_k = (\Delta\nu/\nu)^2\, mc^2/8k\ \ln 2$ where $\Delta\nu$ is the Gaussian linewidth (FWHM), ν is the optical frequency, m is the atomic mass, and k is the Boltzmann constant. Fig. 6a provides the measured time evolution of T_k for different Ar pressures. The variation in T_k with pressure is shown in Fig. 6b, for t=3 μs (corresponding to an early time in the plasma evolution) and also averaged over a time window later in the plasma evolution during which conditions are changing less rapidly. The time window selected depended on the pressure due to the different dynamics. For 1 Torr: Δt'=400-500 μs, 6 Torr: Δt'=400-500 μs, 14 Torr: Δt'=50-100 μs, 45 Torr: Δt'=20-50 μs, and for 100 Torr: Δt'=10-20 μs. The measured temperature shows the expected trend of highest values at early times, followed by a decrease for all background pressures. The T_k values are also highest for higher background pressures at both early and late times in the plasma evolution.

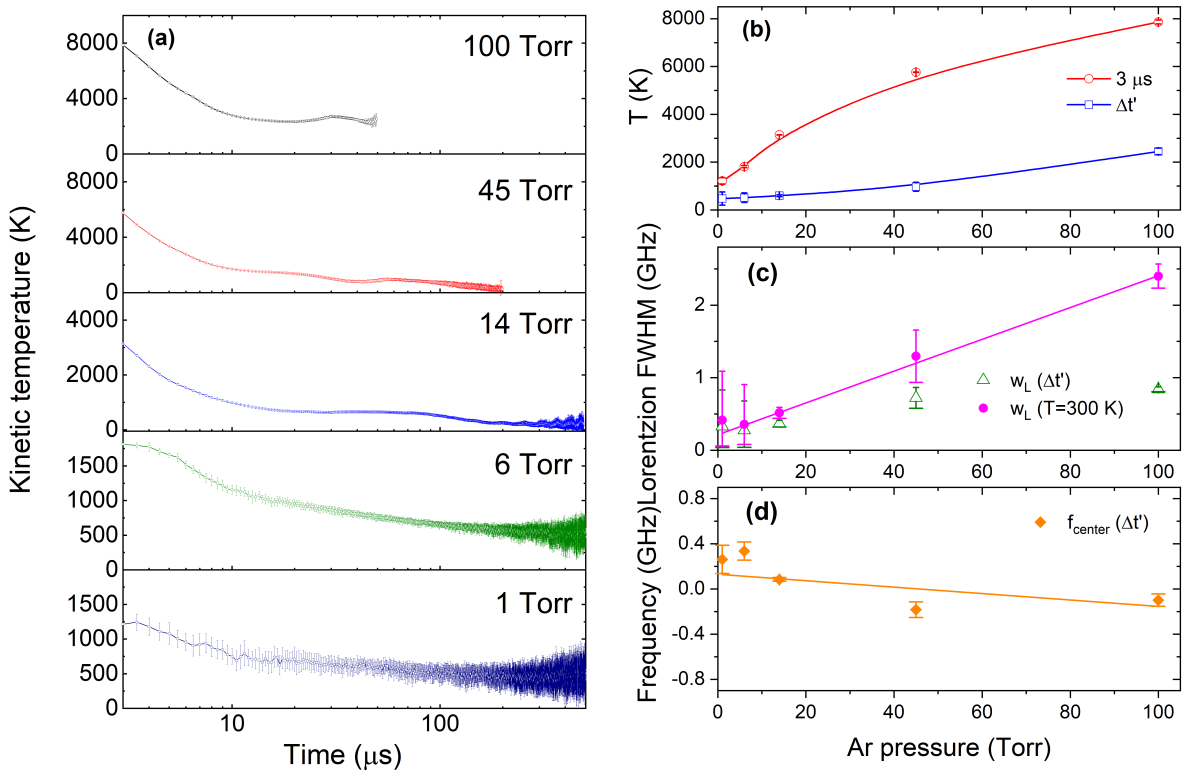

Fig. 6. (a) Kinetic temperature with time for various Ar pressures. (b) Kinetic temperature as a function of Ar pressure for t=3 μs (red circles) and averaged over a time window Δt' later in the evolution (blue squares), where t' depends on the pressure: 1 Torr: Δt'=400-500 μs, 6 Torr: Δt'=400-500 μs, 14 Torr: Δt'=50-100 μs, 45 Torr: Δt'=20-50 μs, 100 Torr: Δt'=10-20 μs. Lines are guides for the eye. (c) Lorentzian linewidth versus pressure averaged over Δt' (green triangles), and after scaling to T=300 K as described in the text (magenta circles). Solid line is a linear fit. (d) Shift of center frequency of peak averaged over Δt' after scaling to

Fig. 6c shows the Lorentzian width (FWHM) determined from the Voigt fits, also averaged over the time windows Δt'. Time windows Δt' were selected later in the plasma evolution to avoid Stark broadening contributions, and during which the fit parameters were not changing rapidly. As expected, the Lorentzian linewidth increases with pressure due to increased van der Waals broadening from collisions with the Ar buffer gas; however, the behavior is not linear with pressure. The nonlinear dependence results because the measurements correspond to different temperatures, as indicated by the data in Fig. 6b.

The increase in Lorentzian linewidth w_L due to van der Waals broadening depends on both pressure p and temperature T via the relationship: $w_L = \gamma_0 \cdot p \cdot (T/T_0)^{0.5}$ where γ_0 is the broadening coefficient determined at a reference temperature T_0 [40]. Although the exponent may vary, we use the standard 0.5 derived from ideal gas law considerations. Fig. 6c shows the Lorentzian linewidths after scaling to a common temperature of T_0=300 K using the above equation: $w_L(300K) = w_L(T) \cdot (T/300)^{0.5}$, where T was taken from the data in Fig. 6b. Fig. 6c also shows a linear fit to the data, and the slope provides the pressure broadening coefficient γ_0=21.9±0.4 MHz/Torr (FWHM) for T=300 K. Fig. 6d shows results from a similar treatment of the shift in the center position of the Al peak versus pressure, from which a pressure shift coefficient of -3±1 MHz/Torr was determined, where the negative sign indicates a shift to lower frequency with increasing pressure. These values are in excellent agreement with

prior measurements on the Al I 394.4 nm transition in Ar, which reported a van der Waals broadening coefficient of 20.2 MHz/Torr (FWHM) and shift coefficient of -3.9 MHz/Torr, with a reported accuracy of 25% [41].

The Al absorption spectral features, kinetic temperature, and column density evolution with time, as well as changing ambient pressure, show a very complex picture of ultrafast LPP dynamics. Although the peak magnitude of absorption increases significantly at higher background pressures, absorbance decays rapidly compared to lower background pressure levels. The change in peak absorbance, as well as persistence with time for various Ar pressures can be attributed to confinement effects. LPPs expand freely in a vacuum and low-pressure background environment when the mean free path of the background gas is significantly larger than the Debye length. Previous studies employing emission spectroscopy of laser plasmas in Ar ambient showed that the plasma plume becomes collisional when the Ar pressure ≥ 0.2 Torr [42]. The 2D TRAS map recorded at 1.1 Torr showed that the absorbance persisted for ≥ 500 μs, although peak absorbance ≤ 0.2. The confinement of the plume typically seen with increasing pressure using OES [43] is also evident in absorption maps (Fig. 2). From geometrical considerations, we expect the measured column density to increase for smaller plasma sizes (~ $1/r^2$ dependence), which is consistent with the measurements presented here.

It is well documented that plasma properties (temperature, density, etc.) change significantly with time and background pressure [9]. The presence of a background gas during laser-produced plasma expansion leads to cooling and thermalization, and it depends strongly on the buffer gas pressure (Fig. 6.). The kinetic temperature measurement using Doppler broadened Al transition shows the cooling effect. Tarallo et al. [44] modeled the temperature decay assuming elastic collisions between two hard spheres (ablated species and buffer gas atoms) and obtained a good agreement with translational temperature. The recorded spectral lines are broadened at early times of plasma evolution regardless of the background pressure (Fig. 2). The high temperatures at early times result in increased linewidths through Doppler broadening. The Lorentzian widths of the Al I transition at early times are expected to be increased due to Stark broadening, with increased broadening at higher pressures due to higher electron density [45,46]; however, in the data measured here the Lorentzian linewidths could not be determined reliably at the earliest times of plasma evolution for lower pressures due to the presence of large spatial gradients and clear deviations from a Voigt lineshape. The measured FWHM are ~17 GHz and ~ 3.2 GHz at times ~1.5 μs and ~2 μs for 100 Torr Ar pressure and based on the impact parameters given in ref. [47], place an upper bound on the respective electron density values at 1.0×10^{16} cm^{-3} and 2.0×10^{15} cm^{-3}. These estimated values are consistent with reported electron densities from those determined via emission spectroscopy of fs LPPs [9]. At later times when the plasma cools and the electron density is negligible, the linewidth results from a combination of Doppler and van der Waals broadening from collisions with the Ar buffer gas. The data in Fig. 6c shows the expected increase in van der Waals broadening with increasing pressure, and a linear dependence after accounting for temperature differences. The ability to measure the van der Waals broadening coefficient accurately in the fs ablation system indicates that at late times the plasma has reached a quasi-static equilibrium with the Ar buffer gas. However, the time and corresponding temperature at which this equilibrium is reached depends strongly on the Ar pressure.

The time at which the column density reaches its maximum values is found to be shifted to later times with increasing pressure (Fig. 2f). This shift can be correlated to an increase in plasma temperature due to plume confinement. The kinetic temperature (T_k) of the plasma is increased significantly at early times with increasing pressure, which decreases the lower level population through excitation. The selected Al transition is a resonance line, and a Boltzmann analysis (not given) shows a rapid decrease of the lower state population when the excitation temperature $T_{ex} \gtrsim 8500\ K$. The measured T_k at early times is consistent with reported excitation temperatures of ultrafast LPP under approximately similar conditions [42]. The kinetic temperature in Fig. 6 is measured from the

Doppler-broadened line profile. Measuring excitation temperature using line ratios was not practical in the current experiments using LAS due to the limited laser scanning range, which in the present case was ~ 30 GHz.. However, absorption spectroscopy employing broadband sources such as arc lamps and frequency combs is useful for temperature measurements employing multiple transitions, and could provide a comparison between the kinetic and excitation temperatures [48,49]. It must be noted that the various temperatures in a plasma (kinetic vs. excitation) should be similar only when the plasma is in local thermodynamic equilibrium (LTE). However, even under LTE, previous studies have shown that disparity in measured plasma temperatures may occur due to the inhomogeneous spatial nature of the plasma and line of sight measurement [49-51].

The confinement of the plasma plumes with increasing Ar background pressure explains the increase in temperature and Al atom density. However, the role of filaments formed during fs laser beam transport cannot be avoided with increasing pressure, and it may influence the laser-target coupling and hence ablation efficiency [9]. Previous studies highlighted that laser-target coupling might be reduced for filament ablation compared to focused fs laser pulses due to intensity clamping effects [46]. Yet, our results show that absorbance levels increase with pressure, indicating that if filaments are present, their generation has an insignificant impact on late time plasma dynamics compared to changes in background pressure.

At moderate pressure levels (i.e., 6-15 Torr), a dual peak in the column density versus time is observed. Such oscillatory behavior was also noticed previously for the excited state population of various species in the plume and explained due to different formation mechanisms of the concerned species [52]. Plume splitting is also reported in the ion temporal profiles [53] and fast gated images [43] when the LPP expands into moderate ambient pressures. Comparing the Al column density evolution and absorbance signals, it can be concluded that the ambient gas collisional cooling of excited species may lead to the formation of a delayed component. Measurements of the combined spatial and temporal dependence of absorption may provide additional insights into the complicated dynamics of LPPs.

IV. SUMMARY

In this article, we used TRAS for characterizing ultrafast LA plumes under different ambient conditions, which provided important information on the time evolution of temperature, column density, and intrinsic linewidths. Spectral linewidths are found to decrease rapidly at early times for all background pressures (over the range of 1-100 Torr Ar) due to the rapid cooling of the plasma and decay in electron density. At later times, linewidths are determined primarily by Doppler broadening and van der Waals pressure broadening. The present study highlights that a significant lower state population exists, even at initial times (~ 1 μs) in the ultrafast LPP lifecycle, which explains the presence of molecular emission features typically seen at early times during ultrafast laser ablation plume evolution compared to ns LPP. The measurement of the pressure broadening coefficient highlights that laser absorption spectroscopy analysis of a laser-produced plasma system is a useful tool for measuring fundamental spectroscopic parameters.

ACKNOWLEDGMENTS

This work was supported partly by the Department of Defense, Defense Threat Reduction Agency (HDTRA1-20-2-0001). The content of the information does not necessarily reflect the position or the

policy of the federal government, and no official endorsement should be inferred. Pacific Northwest National Laboratory is a multi-program national laboratory operated by Battelle for the U.S. Department of Energy under Contract DE-AC05-76RL01830.

[1] S. S. Harilal, B. E. Brumfield, N. L. LaHaye, K. C. Hartig, and M. C. Phillips, *Optical spectroscopy of laser-produced plasmas for standoff isotopic analysis*, Applied Physics Reviews **5**, 021301 (2018).
[2] J. P. Singh and S. N. Thakur, *Laser-induced breakdown spectroscopy* (Elesiver, Amsterdam, 2020).
[3] B. N. Chichkov, C. Momma, S. Nolte, F. vonAlvensleben, and A. Tunnermann, *Femtosecond, picosecond and nanosecond laser ablation of solids*, Appl. Phys. A **63**, 109 (1996).
[4] T. A. Labutin, V. N. Lednev, A. A. Ilyin, and A. M. Popov, *Femtosecond laser-induced breakdown spectroscopy*, J. Anal. Atom. Spectrosc. **31**, 90 (2016).
[5] S. Sunku, M. K. Gundawar, A. K. Myakalwar, P. P. Kiran, S. P. Tewari, and S. V. Rao, *Femtosecond and nanosecond laser induced breakdown spectroscopic studies of NTO, HMX, and RDX*, Spectrochimica Acta Part B: Atomic Spectroscopy **79**, 31 (2013).
[6] E. G. Gamaly, A. V. Rode, B. Luther-Davies, and V. T. Tikhonchuk, *Ablation of solids by femtosecond lasers: Ablation mechanism and ablation thresholds for metals and dielectrics*, Phys. Plasmas **9**, 949 (2002).
[7] A. De Giacomo, M. Dell'Aglio, R. Gaudiuso, S. Amoruso, and O. De Pascale, *Effects of the background environment on formation, evolution and emission spectra of laser-induced plasmas*, Spectrochim. Acta B **78**, 1 (2012).
[8] S. Amoruso, B. Toftmann, and J. Schou, *Thermalization of a UV laser ablation plume in a background gas: From a directed to a diffusionlike flow*, Phys. Rev. E **69**, 056403, 056403 (2004).
[9] E. J. Kautz, J. Yeak, B. E. Bernacki, M. C. Phillips, and S. S. Harilal, *The role of ambient gas confinement, plasma chemistry, and focusing conditions on emission features of femtosecond laser-produced plasmas* Journal of Analytical Atomic Spectrometry **35**, 1574 (2020).
[10] P. J. Skrodzki, M. Burger, I. Jovanovic, M. C. Phillips, B. E. Brumfield, J. Yeak, and S. S. Harilal, *Plume dynamics and gas-phase molecular formation in transient laser-produced U plasmas*, Physics of Plasmas **26**, 083508 (2019).
[11] E. J. Kautz, P. Skrodzki, M. Burger, I. Jovanovic, B. E. Bernacki, M. C. Phillips, and S. S. Harilal, *Time-resolved imaging of atoms and molecules in laser-produced uranium plasmas*, Journal of Analytical Atomic Spectrometry **34**, 2236 (2019).
[12] H. J. Kunze, *Introduction to Plasma Spectroscopy* (Springer Series on Atomic, Optical, and Plasma Physics, 2009), Vol. 56.
[13] J. Scheers, R. Schupp, R. Meijer, W. Ubachs, R. Hoekstra, and O. O. Versolato, *Time- and space-resolved optical Stark spectroscopy in the afterglow of laser-produced tin-droplet plasma*, Phys. Rev. E **102**, 013204, 013204 (2020).
[14] S. Gurlui, M. Agop, P. Nica, M. Ziskind, and C. Focsa, *Experimental and theoretical investigations of a laser-produced aluminum plasma*, Phys. Rev. E **78**, 026405, 026405 (2008).
[15] S. S. Harilal, M. S. Tillack, B. O'Shay, C. V. Bindhu, and F. Najmabadi, *Confinement and dynamics of laser-produced plasma expanding across a transverse magnetic field*, Physical Review E **69**, 026413, 026413 (2004).
[16] J. Bergevin, T.-H. Wu, J. Yeak, B. E. Brumfield, S. S. Harilal, M. C. Phillips, and R. J. Jones, *Dual-Comb Spectroscopy of Laser-Induced Plasmas*, Nature Communications **9**, 1273 (2018).
[17] M. C. Phillips, B. E. Brumfield, N. L. LaHaye, S. S. Harilal, K. C. Hartig, and I. Jovanovic, *Two-dimensional fluorescence spectroscopy of uranium isotopes in femtosecond laser ablation plumes*, Scientific Reports **7**, 3784 (2017).
[18] M. Miyabe, M. Oba, H. Iimura, K. Akaoka, Y. Maruyama, H. Ohba, M. Tampo, and I. Wakaida, *Absorption spectroscopy of uranium plasma for remote isotope analysis of next-generation nuclear fuel*, Appl. Phys. A **112**, 87 (2013).
[19] M. Miyabe, M. Oba, H. Iimura, K. Akaoka, Y. Maruyama, H. Ohba, M. Tampo, and I. Wakaida, *Laser ablation absorption spectroscopy for remote analysis of uranium*, Hyperfine Interactions **216**, 71 (2013).
[20] N. R. Taylor and M. C. Phillips, *Differential laser absorption spectroscopy of uranium in an atmospheric pressure laser-induced plasma*, Optics Letters **39**, 594 (2014).

[21] L. A. King, I. B. Gornushkin, D. Pappas, B. W. Smith, and J. D. Winefordner, *Rubidium isotope measurements in solid samples by laser ablation-laser atomic absorption spectroscopy*, Spectrochim. Acta Part B **54**, 1771 (1999).
[22] R. Stefanuik, E. Sokell, E. Long, N. Krstulovic, P. Hayden, M. Mahmoad, G. O'Sullivan, and P. Dunne, *4d and 5p photoabsorption in laser-produced thulium plasmas*, Physical Review A **101**, 033404 (2020).
[23] J. A. Merten, C. A. Jones, and P. D. Tribbett, *Argon fluoride LA-LEAF for rapid arsenic quantitation*, J. Anal. Atom. Spectrosc. **32**, 1697 (2017).
[24] M. Miyabe, M. Oba, K. Jung, H. Iimura, K. Akoka, M. Kato, H. Otobe, A. Khumaeni, and I. Wakaida, *Laser ablation absorption spectroscopy for isotopic analysis of plutonium: Spectroscopic properties and analytical performance*, Spectrochim. Acta B **134**, 42 (2017).
[25] S. Amoruso, R. Bruzzese, N. Spinelli, and R. Velotta, *Characterization of laser-ablation plasmas*, Journal of Physics B-Atomic Molecular and Optical Physics **32**, R131 (1999).
[26] P. Sankar, J. J. J. Nivas, N. Smijesh, G. K. Tiwari, and R. Philip, *Optical emission and dynamics of aluminum plasmas produced by ultrashort and short laser pulses*, J. Anal. Atom. Spectrosc. **32**, 1177 (2017).
[27] S. A. Kalam, N. L. Murthy, P. Mathi, N. Kommu, A. K. Singh, and S. V. Rao, *Correlation of molecular, atomic emissions with detonation parameters in femtosecond and nanosecond LIBS plasma of high energy materials*, J. Anal. Atom. Spectrosc. **32**, 1535 (2017).
[28] D. Wu, L. Zhang, P. Liu, L. Y. Sun, R. Hai, and H. B. Ding, *Diagnostic study of laser-produced tungsten plasma using optical emission spectroscopy and time-of-flight mass spectroscopy*, Spectrochim. Acta B **137**, 70 (2017).
[29] J. Filevich, J. Grava, M. Purvis, M. C. Marconi, J. J. Rocca, J. Nilsen, J. Dunn, and W. R. Johnson, *Prediction and observation of tin and silver plasmas with index of refraction greater than one in the soft x-ray range*, Phys. Rev. E **74**, 016404, 016404 (2006).
[30] M. Chen, X. D. Liu, M. W. Zhao, C. S. Chen, and B. Y. Man, *Temporal and spatial evolution of Si atoms in plasmas produced by a nanosecond laser ablating silicon carbide crystals*, Phys. Rev. E **80**, 016405, 016405 (2009).
[31] J. Hermann, D. Grojo, E. Axente, C. Gerhard, M. Burger, and V. Craciun, *Ideal radiation source for plasma spectroscopy generated by laser ablation*, Phys. Rev. E **96**, 053210, 053210 (2017).
[32] B. A. Bushaw and M. L. Alexander, *Investigation of laser ablation plume dynamics by high-resolution time-resolved atomic absorption spectroscopy*, Appl. Surf. Sci. **127**, 935 (1998).
[33] H. Liu, A. Quentmeier, and K. Niemax, *Diode laser absorption measurement of uranium isotope ratios in solid samples using laser ablation*, Spectrochimica Acta Part B-Atomic Spectroscopy **57**, 1611, Pii s0584-8547(02)00105-2 (2002).
[34] R. L. Kurucz, Atomic spectral line database, http://www.pmp.uni-hannover.de/cgi-bin/ssi/test/kurucz/sekur.html.
[35] S. S. Harilal, C. M. Murzyn, M. C. Phillips, and J. B. Martin, *Hyperfine structures and isotopic shifts of uranium transitions using tunable laser spectroscopy of laser ablation plumes* Spectrochimica Acta B **169**, 105828 (2020).
[36] P. J. Skrodzki, N. Shah, N. Taylor, K. Hartig, N. LaHaye, B. Brumfield, I. Jovanovic, M. C. Phillips, and S. S. Harilal, *Significance of plasma-ambient conditions in U absorption and emission features in laser ablation plasmas*, Spectrochimica Acta Part B-Atomic Spectroscopy **125** 112 (2016).
[37] O. Axner, J. Gustafsson, N. Omenetto, and J. D. Winefordner, *Line strengths, A-factors and absorption cross-sections for fine structure lines in multiplets and hyperfine structure components in lines in atomic spectrometry - a user's guide*, Spectrochim. Acta B **59**, 1 (2004).
[38] E. S. Chang, *Energy-Levels of Atomic Aluminum with Hyperfine-Structure*, J Phys Chem Ref Data **19**, 119 (1990).
[39] N. Konjevic, *Plasma broadening and shifting of non-hydrogenic spectral lines; Present status and applications*, Physics Reports-Review Section of Physics Letters **316**, 339 (1999).
[40] W. Demtroder, *Laser Spectroscopy 2, Experimental methods* (Springer, Heidelberg, 2015), 2.
[41] G. Rondigs and H. J. Kusch, *Broadening and Shift of Neutral Aluminum Lines by Van-Der-Waals-Interaction with Argon and Helium-Atoms*, Astron Astrophys **70**, 151 (1978).
[42] P. K. Diwakar, S. S. Harilal, M. C. Phillips, and A. Hassanein, *Characterization of ultrafast laser-ablation plasma plumes at various Ar ambient pressures*, J. Appl. Phys. **118**, 043305 (2015).
[43] S. S. Harilal, C. V. Bindhu, M. S. Tillack, F. Najmabadi, and A. C. Gaeris, *Internal structure and expansion dynamics of laser ablation plumes into ambient gases*, J. Appl. Phys. **93**, 2380 (2003).

[44] M. Tarallo, G. Iwata, and T. Zelevinsky, *BaH molecular spectroscopy with relevance to laser cooling*, Physical Review A **93**, 032509 (2016).
[45] E. J. Kautz, J. Yeak, B. E. Bernacki, M. C. Phillips, and S. S. Harilal, *Expansion dynamics and chemistry evolution in ultrafast laser filament produced plasmas* Physical Chemistry Chemical Physics **21**, 16161 (2020).
[46] S. S. Harilal, J. Yeak, B. E. Brumfield, and M. C. Phillips, *Consequences of femtosecond laser filament generation conditions in standoff LIBS* Optics Express **24**, 17941 (2016).
[47] N. Konjevic and W. L. Wiese, *Experimental stark widths and shifts for spectral-lines of neutral and ionized atoms*, Journal of Physical and Chemical Reference Data **19**, 1307 (1990).
[48] Y. Zhang, C. Lecaplain, R. R. D. Weeks, J. Yeak, S. S. Harilal, M. C. Phillips, and R. J. Jones, *Time-Resolved Dual-Comb Measurement of Number Density and Temperature in a Laser-Induced Plasma*, Opt. Lett. **44**, 3458 (2019).
[49] E. N. Weerakkody, D. G. Weisz, J. Crowhurst, B. Koroglu, T. Rose, H. Radousky, R. L. Stillwell, J. R. Jeffries, and N. G. Glumac, *Time-resolved formation of uranium and silicon oxides subsequent to the laser ablation of U3Si2,*, Spectrochimica Acta Part B: Atomic Spectroscopy **170**, 105925 (2020).
[50] J. A. Aguilera and C. Aragon, *Characterization of a laser-induced plasma by spatially resolved spectroscopy of neutral atom and ion emissions. Comparison of local and spatially integrated measurements*, Spectrochim. Acta B **59**, 1861 (2004).
[51] N. L. LaHaye, S. S. Harilal, and M. C. Phillips, *Early- and late-time dynamics of laser-produced plasmas by combining emission and absorption spectroscopy*, Spectrochimica Acta B, in press (2021).
[52] S. S. Harilal, R. C. Issac, C. V. Bindhu, V. P. N. Nampoori, and C. P. G. Vallabhan, *Emission characteristics and dynamics of C-2 from laser produced graphite plasma*, J. Appl. Phys. **81**, 3637 (1997).
[53] C. Focsa, S. Gurlui, P. Nica, M. Agop, and M. Ziskind, *Plume splitting and oscillatory behavior in transient plasmas generated by high-fluence laser ablation in vacuum*, Appl. Surf. Sci. **424**, 299 (2017).